# Rigorous supermode solutions in a strong absorption slab waveguide and application to design of a waveguide photodetector

**Xuecai Yu (余学才)*, Yanxi Gu (古燕西), Daiyao Chen (陈代尧), Xiaogang Zhang (张晓刚), and Yong Liu (刘 永)**

*School of Optic and Electronic Message, Electronic Science and Technology of China, Chengdu 610054, China*

**Corresponding author: yxc@uestc.du.cn*

Received January 29, 2013; accepted March 29, 2013; posted online May 31, 2013

A rigorous supermode solution method in a strong absorption slab multilayer waveguide is performed. The method is directed toward finding solutions for a sophisticated complex determinant in a complex plane. The rigorous results are applied to design a waveguide photodetector that has a configuration of a vertical directional coupler. Absorption lengths of the supermodes and coupling length of the coupler are calculated based on an effective index approach by using the rigorous results of the strong absorption slab multilayer waveguide to optimize the directional coupling waveguide photodetector.

*OCIS codes:* 130.130, 040.0040, 230.0230.
*doi: 10.3788/COL201311.061301.*

Optical amplification and absorption in a medium can be described by a complex refractive index $n = n_{\rm R} \pm {\rm j}n_{\rm I}$, where the imaginary part $n_{\rm I}$ represents amplification (+sign) or absorption (-sign). Intrinsically, a semiconductor works as a strong gain waveguide, and an InGaAs waveguide photodetector has a strong absorption ability[1−5].

Amplification or absorption has been proven to affect waveguide modes experimentally and theoretically. For example, a gain in GaN laser may cause a lasing mode to shift out of the gain region, thus extinguishing the lasing process[6]. Such mode is called ghost mode. From a mathematical point of view, the wave equation in an absorption medium becomes a damping equation in which intrinsic solutions are no longer orthogonal to each other[7]. An excessively large absorption or gain results in the invalidation of such algorithms for mode recognition, as in Beam prop software of RSoft Design Group.

This letter demonstrates a rigorous method that can be used to solve supermodes in a strong absorption slab waveguide with multilayers. Such method is applicable to waveguides with arbitrary absorption and amplification. Moreover, an exemplary application designs an InGaAs waveguide photodetector with the configuration of a vertical directional coupler.

An InGaAs waveguide photodetector has the architecture of a directional coupler[8]. Waveguide photodetectors have been studied for years in radio-over-fiber (ROF) applications, where the detectors require high power and fast speed. To reduce possible overheating in front of the waveguide, a directional coupling waveguide photodiode was proposed in this research. Figure 1 shows the directional coupler of interest as two InGaAsP waveguides (upper and lower) on both sides of an InP layer. An InGaAs absorption layer for a 1.55-$\mu$m wavelength sits on the top of the upper waveguide. A light beam incident to the lower waveguide is gradually coupled with the upper waveguide. Other extensive studies have shown[9] that the absorption length of the fundamental supermode $l_{\rm ab,0}$, the absorption length of the first supermode $l_{\rm ab,1}$, and the coupling length $l_{\rm c}$ should be equal to each other to gain the highest level of electric current distribution. These lengths are determined from complex propagating constants of the fundamental and first super-orders $\beta_0 = (2\pi/\lambda)n_{\rm eff,0}$ and $\beta_1 = (2\pi/\lambda)n_{\rm eff,1}$ by

$$\begin{cases} l_{\rm ab,\,0} = \frac{\lambda}{4\pi {\rm Im}(n_{\rm eff,0})} \\ l_{\rm ab,\,1} = \frac{\lambda}{4\pi {\rm Im}(n_{\rm eff,1})} \\ l_{\rm c} = \frac{\lambda}{2{\rm Re}(n_{\rm eff,0} - n_{\rm eff1})} \end{cases}, \tag{1}$$

where $n_{\rm eff,0}$ and $n_{\rm eff,1}$ represent the effective indices of the two modes. The complex propagating constants of the fundamental and first-order modes for a particular structure of the coupler have a crucial role in the optimization of the directional coupling waveguide photodetector.

An electric field $E_y(x)$ of TE guiding modes in the slab waveguide shown in Fig. 1 can be written as

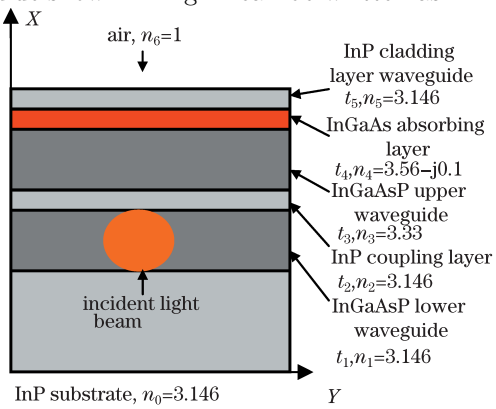


Fig. 1. Structure of the one-dimensional (1D) slab waveguide photodetector with seven layers.

 

$$\begin{cases} E_y(x,z) = A_m(\xi_1+\xi_2)\exp(\gamma_1 x)\exp(-\mathrm{j}\beta_m z) \quad (x \leqslant 0) \\ E_y(x,z) = A_m[\xi_1\exp(\gamma_2 x)+\xi_2\exp(-\gamma_2 x)]\exp(-\mathrm{j}\beta_m z) \quad (0 \leqslant x \leqslant t_1) \\ E_y(x,z) = A_m[\xi_3\exp(\gamma_3(x-t_1)]+\xi_4\exp[-\gamma_3(x-t_1)]\exp(-\mathrm{j}\beta_m z) \quad (t_1 \leqslant x \leqslant t_1+t_2) \\ E_y(x,z) = A_m\left\{\xi_5\exp[\gamma_4(x-t_1-t_2)]+\xi_6\exp[-\gamma_4(x-t_1-t_2)]\right\}\exp(-\mathrm{j}\beta_m z) \quad (t_1+t_2 \leqslant x \leqslant t_1+t_2+t_3) \\ E_y(x,z) = A_m\left\{\xi_7\exp[\gamma_5(x-t_1-t_2-t_3)]+\xi_8\exp[-\gamma_5(x-t_1-t_2-t_3)]\right\}\exp(-\mathrm{j}\beta_m z) \\ (t_1+t_2+t_3 \leqslant x \leqslant t_1+t_2+t_3+t_4+t_5) \\ E_y(x,z) = A_m\left\{\xi_9\exp[\gamma_6(x-t_1-t_2-t_3-t_4))+\xi_{10}\exp(-\gamma_6(x-t_1-t_2-t_3-t_4)]\right\}\exp(-\mathrm{j}\beta_m z) \\ (t_1+t_2+t_3+t_4 \leqslant x \leqslant t_1+t_2+t_3+t_4+t_5) \\ E_y(x,z) = A_m[\xi_9\exp(\gamma_6 t_5)+\xi_{10}\exp(-\gamma_6 t_5)]\exp[-\gamma_7(x-t_1-t_2-t_3-t_4-t_5)]\exp(-\mathrm{j}\beta_m z) \\ (x \geqslant t_1+t_2+t_3+t_4+t_5) \end{cases}, \quad (2)$$

where $A_m$ is a constant, $\xi_i$ ($i$=1, 2, 3, 4, 5, 6, and 7) are constants determined by boundary conditions, $t_i$ is the thickness of the $i$th layer, $\beta_m = n_{\mathrm{e},m}2\pi/\lambda$ is the propagating constant of the $m$th mode, $n_{\mathrm{e},m} = n_{\mathrm{R},m} - \mathrm{j}n_{\mathrm{I},m}$ is the complex effective refractive index, $\lambda$ is the vacuum wavelength of the light, and

$$\gamma_i = \sqrt{\beta_m^2 - n_i^2 2\pi/\lambda}. \quad (3)$$

The continuity of $E_y(x)$ and $\partial E_y(x)/\partial x$ at the interfaces satisfies a characteristic equation:

$$\det\begin{bmatrix} e^{\gamma_2 t_1} & e^{-\gamma_2 t_1} & -1 & -1 & 0 & 0 & 0 & 0 & 0 & 0 \\ 0 & 0 & e^{\gamma_3 t_2} & e^{-\gamma_3 t_2} & -1 & -1 & 0 & 0 & 0 & 0 \\ 0 & 0 & 0 & 0 & e^{\gamma_4 t_3} & e^{-\gamma_4 t_3} & -1 & -1 & 0 & 0 \\ 0 & 0 & 0 & 0 & 0 & 0 & e^{\gamma_5 t_4} & e^{-\gamma_5 t_4} & -1 & -1 \\ \gamma_1-\gamma_2 & \gamma_1+\gamma_2 & 0 & 0 & 0 & 0 & 0 & 0 & 0 & 0 \\ \gamma_2 e^{\gamma_2 t_1} & -\gamma_2 e^{-\gamma_2 t_1} & -\gamma_3 & \gamma_3 & 0 & 0 & 0 & 0 & 0 & 0 \\ 0 & 0 & \gamma_3 e^{\gamma_3 t_2} & -\gamma_3 e^{-\gamma_3 t_2} & -\gamma_4 & \gamma_4 & 0 & 0 & 0 & 0 \\ 0 & 0 & 0 & 0 & \gamma_4 e^{\gamma_4 t_3} & -\gamma_4 e^{-\gamma_4 t_3} & -\gamma_5 & \gamma_5 & 0 & 0 \\ 0 & 0 & 0 & 0 & 0 & 0 & \gamma_5 e^{\gamma_5 t_4} & -\gamma_5 e^{-\gamma_5 t_4} & -\gamma_6 & \gamma_6 \\ 0 & 0 & 0 & 0 & 0 & 0 & 0 & 0 & (\gamma_6+\gamma_7)e^{\gamma_6 t_5} & (\gamma_7-\gamma_6)e^{-\gamma_6 t_5} \end{bmatrix} = 0. \quad (4)$$

A similar characteristic equation for TM mode has the same form:

$$\det\begin{bmatrix} e^{\nu_2 t_1} & e^{-\nu_2 t_1} & -1 & -1 & 0 & 0 & 0 & 0 & 0 & 0 \\ 0 & 0 & e^{\nu_3 t_2} & e^{-\nu_3 t_2} & -1 & -1 & 0 & 0 & 0 & 0 \\ 0 & 0 & 0 & 0 & e^{\nu_4 t_3} & e^{-\nu_4 t_3} & -1 & -1 & 0 & 0 \\ 0 & 0 & 0 & 0 & 0 & 0 & e^{\nu_5 t_4} & e^{-\nu_5 t_4} & -1 & -1 \\ \frac{\nu_1}{n_1^2}-\frac{\nu_2}{n_2^2} & \frac{\nu_1}{n_1^2}+\frac{\nu_2}{n_2^2} & 0 & 0 & 0 & 0 & 0 & 0 & 0 & 0 \\ e^{\nu_2 t_1} & -e^{-\nu_2 t_1} & -\frac{\nu_3}{\nu_2}\frac{n_2^2}{n_3^2} & \frac{\nu_3}{\nu_2}\frac{n_2^2}{n_3^2} & 0 & 0 & 0 & 0 & 0 & 0 \\ 0 & 0 & e^{\nu_3 t_2} & -e^{-\nu_3 t_2} & -\frac{\nu_4}{\nu_3}\frac{n_3^2}{n_4^2} & \frac{\nu_4}{\nu_3}\frac{n_3^2}{n_4^2} & 0 & 0 & 0 & 0 \\ 0 & 0 & 0 & 0 & e^{\nu_4 t_3} & -e^{-\nu_4 t_3} & -\frac{\nu_5}{\nu_4}\frac{n_4^2}{n_5^2} & \frac{\nu_5}{\nu_4}\frac{n_4^2}{n_5^2} & 0 & 0 \\ 0 & 0 & 0 & 0 & 0 & 0 & e^{\nu_5 t_4} & -e^{-\nu_5 t_4} & -\frac{\nu_6}{\nu_5}\frac{n_5^2}{n_6^2} & \frac{\nu_6}{\nu_5}\frac{n_5^2}{n_6^2} \\ 0 & 0 & 0 & 0 & 0 & 0 & 0 & 0 & (1+\frac{\nu_7}{\nu_6}\frac{n_6^2}{n_7^2})e^{\nu_6 t_5} & (-1+\frac{\nu_7}{\nu_6}\frac{n_6^2}{n_7^2})e^{-\nu_6 t_5} \end{bmatrix} = 0, \quad (5)$$

where $\nu_i = \sqrt{\beta_m^2 - n_i^2 2\pi/\lambda}$. The characteristic Eqs. (4) and (5) are complex determinant equations. Both their real and imaginary parts of the determinate must vanish:

$$\det(H) = H_{\mathrm{R}} - \mathrm{j}H_{\mathrm{I}} = 0. \quad (6)$$

The $m$th root of the characteristic equations results in a complex effective index $n_{\mathrm{e},m} = n_{\mathrm{R},m} - \mathrm{j}n_{\mathrm{I},m}$ of the $m$th mode, which can be found by searching particular points in an entire complex plane.

A conventional algorithm to find a solution to Eq. (4) or Eq. (5) includes the assumption of an arbitrary trial quantity of the effective index $n_{\mathrm{e}} = n_{\mathrm{R}} - \mathrm{j}n_{\mathrm{I}}$, substitution of the trial quantity into the characteristic equation, and modification of the assumption if Eq. (4) (TE mode) or Eq. (5) (TM mode) is not satisfied. The algorithm does not take the trial quantity as one root until Eq. (4) is satisfied. However, such algorithm appears to be inefficient because the sophisticated characteristic equations have smart sensibility for a trial quantity. The special computing flow shown in Fig. 2 is recommended for a quick and precise search of the complex roots without

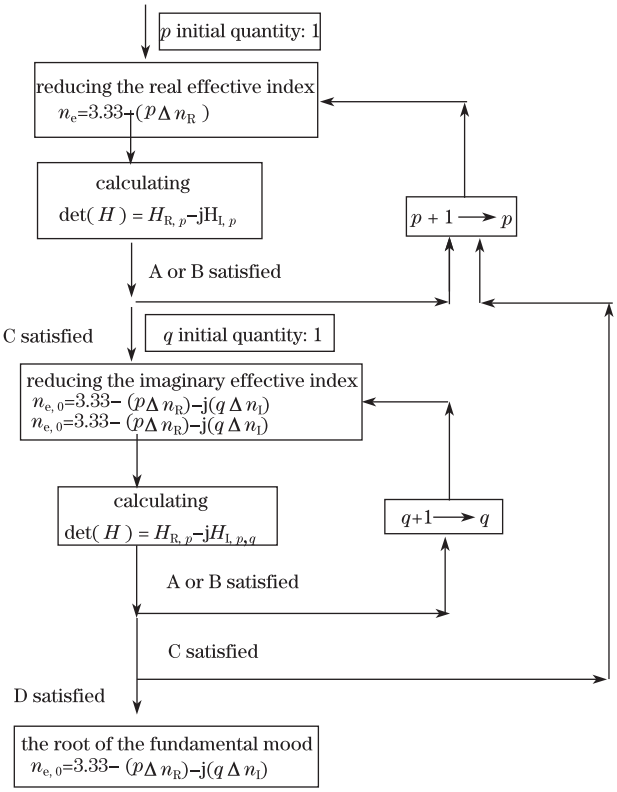


Fig. 2. Flowchart used to calculate the roots of the characteristic equation.

missing any possible roots.

The range of the trial value of the real effective index should be from the InP cladding layer index of 3.146 to the InGaAsP guiding layer index of 3.33. Steps of effective indices $\Delta n_{\rm R}$ and $\Delta n_{\rm I}$ have to be sufficiently small to ensure that no roots can possibly be lost. The four switch conditions A, B, C, and D in Fig. 2 indicate the following concepts:

A. The larger part of the absolutions of $H_{\rm R}$ and $H_{\rm I}$ decreases as the effective indices $n_{\rm R}$ and $n_{\rm I}$ change:

$$\max(|H_{{\rm R},n+1}|,|H_{{\rm I},n+1}|)-\max(|H_{{\rm R},n}|,|H_{{\rm I},n}|)<0.$$

B. The absolutions of $H_{\rm R}$ and $H_{\rm I}$ are simultaneously reduced as the effective indices $n_{\rm R}$ and $n_{\rm I}$ change:

$$\begin{aligned}&|H_{{\rm R},n+1}|-|H_{{\rm R},n}|<0,\\&|H_{{\rm I},n+1}|-|H_{{\rm I},n}|<0.\end{aligned}$$

C. The absolutions of $H_{\rm R}$ and $H_{\rm I}$ are very close to each other:

$$\frac{|H_{{\rm R},n+1}|-|H_{{\rm I},n+1}|}{|H_{{\rm R},n+1}|+|H_{{\rm I},n+1}|}<0.001.$$

D. The absolutions of $H_{\rm R}$ and $H_{\rm I}$ are small quantities:

**Table 1. Thicknesses of the Layers**

| Layer | $t_0$ | $t_1$ | $t_2$ | $t_3$ | $t_4$ | $t_5$ | $t_6$ |
|---|---|---|---|---|---|---|---|
| Thickness ($\mu$m) | – | 2.80 | 0.09 | 3.00 | 0.08 | 0.80 | – |
| Refractive Index | 3.146 | 3.33 | 3.146 | 3.33 | 3.56-0.1i | 3.146 | 1 |

**Table 2. Effective Indices of Fundamental Supermode and First-order Supermode in the Slab Waveguide**

| | Fundamental Order | First Order |
|---|---|---|
| TE Mode | 3.32523-0.00105i | 3.32271-0.00119i |
| TM Mode | 3.32412-0.00101i | 3.322652-0.00115i |

$$\begin{aligned}&|H_{{\rm R},n+1}|<0.01,\\&|H_{{\rm I},n+1}|<0.01.\end{aligned}$$

Once the fundamental root is found, the first root can be determined by using the fundamental root as a new initial trial value. Higher roots can be obtained successively in the same manner until the real effective index approaches the cladding index of 3.146.

The thickness of each layer and the refractive indices of the multilayer waveguide considered in this letter are listed in Table 1. Table 2 shows the exact effective indices of the fundamental and first modes for both TE and TM modes, computed from the above flow. The field distributions of the TE fundamental and first modes are shown in Figs. 3 and 4. The two modes are approximate linear combinations of modes in the upper and lower individual waveguides, in phase, and out phase, respectively.

To optimize the current distribution in the two-dimensional (2D) directional coupling waveguide photodetector shown in Fig. 5, the propagating constants of the fundamental mode and the first mode should be determined. In the effective index approach, the 2D waveguide in Fig. 5 is equivalent to a 1D slab symmetric waveguide with refractive indices $n_{\rm e,0}$. The complex effective index of the fundamental mode of the 1D waveguide shown in Fig. 1 is solved using the previous procedure.

The TE mode in Fig. 1 must be a TM mode in the equivalent 1D slab symmetric waveguide because the electric field of the TE mode in Fig. 2 lies on the horizontal direction. The electric field direction of the TM mode in the equivalent waveguide is perpendicular to the interfaces. Similarly, the TM mode in Fig. 1 must be a TM mode in the equivalent waveguide.

From the continuity of the field at the interfaces, a charicteristic equation of TM modes in Fig. 5 can be determined by

$$\det\begin{bmatrix} r_1-r_2 & r_1+r_2 \\ (r_1+r_2)\exp(r_2w) & (r_1-r_2)\exp(-r_2w)\end{bmatrix}=0, \tag{7}$$

$$\begin{cases} r_1=k(n_{\rm eff}^2-n_{\rm e,c}^2)^{1/2} \\ r_2=k(n_{\rm eff}^2-n_{\rm e}^2)^{1/2}\end{cases}, \tag{8}$$

where $w$ is the ridge width, and $n_{\rm e,c}$ is the cladding effective index.

The roots of the new complex characteristic Eq. (8) for the 2D directional waveguide photodetector are also precisely calculated by following the flowchart in Fig. 2.

Optimization is accomplished by changing the thicknesses of the upper and lower waveguides to make the absorption lengths of the fundamental and first-order modes

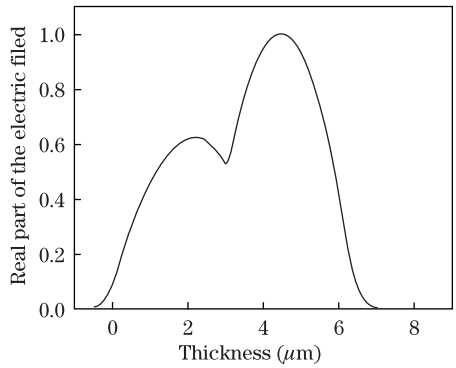


Fig. 3. Field distribution of the TE fundamental mode.

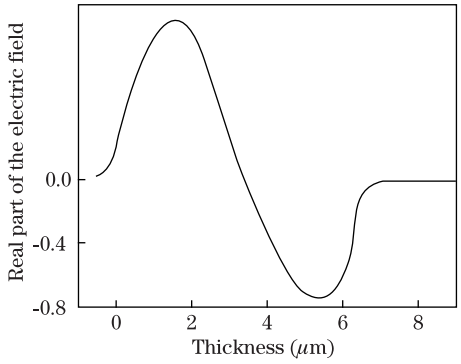


Fig. 4. Field distribution of the TE first mode.

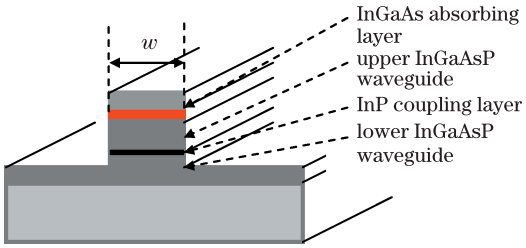


Fig. 5. Structure of the 2D directional waveguide photodetector.

close to each other (not necessarily equal), and then modifying the thickness of the InP layer between the upper and lower waveguides to make the coupling length close to the absorption length. For a 3-$\mu$m ridge width, the optimized results, absorption lengths, and coupling length for $TE_{00}$ and $TE_{01}$, as well as $TM_{00}$ and $TM_{01}$ modes, in the 2D directional coupler are listed in Table 3. The difference between the absorption lengths and coupling lengths are sufficiently small so they can be tolerated from the beam prop simulation of absorption profiles. Notably, the minimal difference between TM and TE modes indicates that this waveguide detector is polarization insensitive.

A precise method that can be used to determine supermodes in a strong absorption multilayer slab waveguide is applied to design a waveguide photodetector with the configuration of a directional coupler. No approximation is made for a 1D slab absorption waveguide. A 1D slab waveguide photodetector should be designed to precisely satisfy optimal conditions by employing a rigorous method. For the 2D directional coupling waveguide photodetector, although field distributions of modes are not

**Table 3. Parameters of $TE_{00}$, $TE_{01}$, $TM_{00}$, and $TM_{01}$($\omega$=3 $\mu$m) in the Directional Coupling Waveguide Photodetector**

| Mode | Complex Index | Effective Absorption Length ($\mu$m) | Coupling Length ($\mu$m) |
|---|---|---|---|
| $TE_{00}$ | 3.235971-0.0003150i | 390 | 370 |
| $TE_{01}$ | 3.233871-0.0002957i | 417 | |
| $TM_{00}$ | 3.236129-0.0003248i | 360 | 378 |
| $TM_{01}$ | 3.233591-0.0003221i | 380 | |

continuous at interfaces within the effective index approach, only the propagating constants of modes are of interest for the optimization. Calculations based on the rigorous method reveal the ghost-mode phenomenon and a more complicated supermode structure. For example, for a thicker InGaAs absorption layer with a higher index of 3.56, the fundamental supermode near the absorption layer is possibly negative because one supermode profile can be roughly understood as a possible continuous link between the individual mode profiles in the lower waveguide, the upper waveguide, and the InGaAs layer. The first-order mode exists in a thicker layer (such as thicker than 0.3 $\mu$m) due to its higher index. The fundamental supermode is nearly composed of the individual fundamental modes in the two waveguides and the individual first mode in the InGaAs layer. To satisfy field continuity, a supermode field in the upper waveguide and near the InGaAs layer is extended to a negative region to link the negative field of the first-order mode in the InGaAs absorption layer. In this case, the supermode is distributed with an unusual distortion. As a result, the absorption is reduced because the average field of the first mode is smaller than that of the fundamental mode in the absorption layer. The reduction of absorption for a thicker absorption layer can be observed from a beam prop simulation, but is easily ignored. Thus, absorption is not proportional to the covering factor.

In conclusion, strong absorption and amplification in a waveguide result in some problems in digital mode recognition. For instance, one algorithm is used to observe a convergent steady distribution of the field pattern as light propagates along a waveguide with symmetric or asymmetric excitation at the front end of the waveguide. A steady fundamental mode and higher-order modes are observed while a waveguide is sufficiently long for symmetric and asymmetric excitations, respectively. However, for a strong absorption and amplification waveguide, the distribution pattern can never be convergent to a steady distribution.

This work was supported by the National Natural Science Foundation of China under Grant Nos. 61177036 and 60925019.

## References

1. K. Kato, A. Kozen, Y. Muramoto, Y. Itaya, T. Nagatsuma, and M. Yaita, IEEE Photon. Technol. Lett. **6,** 719 (1994).
2. J. Klamkin, A. Ramaswamy, L. A. Johansson, H. F. Chou, M. N. Sysak, J. W. Raring, N. Parthasarathy, S. P. Denbaars, J. E. Bowers, and L. A. Coldren, IEEE

Photon. Technol. Lett. **19,** 149 (2007).

3. S. M. Madison, J. Klamkin, D. C. Oakley, A. Napoleone, J. J. Plant, and P. W. Juodawlkis, IEEE Photon. J. **3,** 676 (2011).
4. J. Klamkin, Y. C. Chang, A. Ramassamy, L. A. Johansson, J. E Bowers, S. P. DenBaars, and L. A. Coldren, IEEE J. Quantum Electron. **44,** 354 (2008).
5. P. W. Juodawlkis, J. J. Plant, W. Loh, L. J. Missaggia, F. J. O'Donnell, D. C. Oakley, A. Napoleone, J. Klamkin, J. T. Gopinath, D. J. Ripin, S. Gee, P. J. Delfyett, and J. P. Donnelly, IEEE J. Sel. Top. Quantum Electron. **17,** 1698 (2011).
6. P. G. Eliseev, G. A. Smolyakov, and M. Osinski, IEEE J. Sel. Top. Quantum Electron. **5,** 771 (1999).
7. P. Gerard, Opt. Commun. **151**, 110 (1998).
8. M. N. Draa, J. Bloch, D. Chen, D. C. Scott, N. Chen, S. B. Chen, X. Yu, W. S. Chang, and P. K. L. Yu, Opt. Express **18,** 17729 (2010).
9. X. Yu, in *Proceedings of the 5th SPIE International Symposium on Advanced Optical Manufacturing and Testing Technology* 607 (2010).